

Original citation:

Chapman, Sandra C., Dendy, R. O., Lang, P. T., Watkins, Nicholas W., Calderon, F. A., Romanelli, M. and Todd, T. N.. (2017) The global build-up to intrinsic ELM bursts and comparison with pellet triggered ELMs seen in JET. Nuclear Fusion, 57 (2). 022017.

Permanent WRAP URL:

<http://wrap.warwick.ac.uk/81909>

Copyright and reuse:

The Warwick Research Archive Portal (WRAP) makes this work of researchers of the University of Warwick available open access under the following conditions.

This article is made available under the Creative Commons Attribution 3.0 (CC BY 3.0) license and may be reused according to the conditions of the license. For more details see:

<http://creativecommons.org/licenses/by/3.0/>

A note on versions:

The version presented in WRAP is the published version, or, version of record, and may be cited as it appears here.

For more information, please contact the WRAP Team at: wrap@warwick.ac.uk

The global build-up to intrinsic ELM bursts and comparison with pellet triggered ELMs seen in JET

This content has been downloaded from IOPscience. Please scroll down to see the full text.

2017 Nucl. Fusion 57 022017

(<http://iopscience.iop.org/0029-5515/57/2/022017>)

View [the table of contents for this issue](#), or go to the [journal homepage](#) for more

Download details:

IP Address: 209.93.156.68

This content was downloaded on 30/09/2016 at 18:01

Please note that [terms and conditions apply](#).

The global build-up to intrinsic ELM bursts and comparison with pellet triggered ELMs seen in JET

S.C. Chapman¹, R.O. Dendy^{1,2}, P.T. Lang³, N.W. Watkins^{1,4,5}, F.A. Calderon¹, M. Romanelli², T.N. Todd² and JET Contributors^a

EUROfusion Consortium, JET, Culham Science Centre, Abingdon, OX14 3DB, UK

¹ Centre for Fusion, Space and Astrophysics, Department of Physics, University of Warwick, Coventry, UK

² CCFE, Culham Science Centre, Abingdon, Oxfordshire OX14 3DB, UK

³ Max-Planck-Institut für Plasmaphysik, Garching, Germany

⁴ Centre for the Analysis of Time Series, London School of Economics, London, UK

⁵ Faculty of Mathematics, Computing and Technology, Open University, Milton Keynes, UK

E-mail: S.C.Chapman@warwick.ac.uk

Received 28 January 2016, revised 20 June 2016

Accepted for publication 2 August 2016

Published 30 September 2016



CrossMark

Abstract

We focus on JET plasmas in which ELMs are triggered by pellets in the presence of ELMs which occur naturally. We perform direct time domain analysis of signals from fast radial field coils and toroidal full flux azimuthal loops. These toroidally integrating signals provide simultaneous high time resolution measurements of global plasma dynamics and its coupling to the control system. We examine the time dynamics of these signals in plasmas where pellet injection is used to trigger ELMs in the presence of naturally occurring ELMs. Pellets whose size and speed are intended to provide maximum local perturbation for ELM triggering are launched at pre-programmed times, without correlation to the occurrence times of intrinsic ELMs. Pellet rates were sufficiently low to prevent sustained changes of the underlying plasma conditions and natural ELM behaviour. We find a global signature of the build-up to natural ELMs in the temporal analytic phase of both the full flux loops and fast radial field coil signals. Before a natural ELM, the signal phases align to the same value on a $\sim 2\text{--}5$ ms timescale. This global build up to a natural ELM occurs whilst the amplitude of the full flux loop and fast radial field coil signals are at their background value: it precedes the response seen in these signals to the onset of ELMing. In contrast these signals do not clearly phase align before the ELM for ELMs which are the first to occur following pellet injection. This provides a direct test that can distinguish when an ELM is triggered by a pellet as opposed to occurring naturally. It further supports the idea [1–4] of a global build up phase that precedes natural ELMs; pellets can trigger ELMs even when the signal phase is at a value when a natural ELM is unlikely to occur.

Keywords: edge localised modes, control system, phase synchronization, pellets

(Some figures may appear in colour only in the online journal)

^a See the appendix of [42].



Original content from this work may be used under the terms of the [Creative Commons Attribution 3.0 licence](https://creativecommons.org/licenses/by/3.0/). Any further distribution of this work must maintain attribution to the author(s) and the title of the work, journal citation and DOI.

1. Introduction

Intense, short duration relaxation events known as edge localized modes (ELMs) [5–9] generally accompany enhanced confinement (H-mode) regimes in tokamak plasmas. Mitigation of large amplitude ELMs is essential for ITER because each ELM releases particles and energy which load the plasma facing components; scaled up to ITER [10], the largest such loads would be unacceptable. ELMs also play a role in removing impurities from the plasma, which should also be achieved in a controllable manner. The peeling-ballooning MHD instability at the plasma edge is believed to underlie the onset of an ELM burst [11–14] once local conditions for instability are reached. The sequence of events that leads to this remains an open question.

Empirically, longer waiting times between one ELM and the next broadly correlate with larger ELM amplitudes, so that proposals for mitigation include externally triggering many, smaller ELMs [15–18]. One method is to modify the conditions at the edge by injecting frozen deuterium pellets which quickly ionise [19–24], see also the topical review [25]. Pellet ELM pacing relies on the triggering of an ELM by the strong local perturbation created by the ablated particles deposited in the plasma edge. Whilst previously found to be very effective in a Carbon wall environment, recently it has been found that the triggering efficiency is greatly diminished when changing to an all-metal-wall in JET and ASDEX Upgrade. In particular, lag-times have been observed between pellet injection and subsequent ELM where pellets failed to trigger. Successful triggering conditions depend on some combination of critical plasma and pellet parameters. Investigations of the underlying physics of the process by which pellets can trigger ELMs require the capability to discriminate between successful and unsuccessful attempts to trigger an ELM with an injected pellet. Pellet injection is applied to plasmas where there are frequently occurring natural ELMs and pellets can fail to trigger ELMs. A pellet is injected and then an ELM occurs shortly after but there is a likelihood that this ELM would have occurred even if the pellet had not been injected. An ELM is only known with high confidence to be triggered by a pellet if the pellet is injected when the time that has elapsed since the preceding ELM is much shorter than the typical inter-ELM time for the naturally occurring ELMs, and this may not be realized experimentally [35].

Quantitative characterization of the time domain dynamics of ELMing processes is relatively novel [26–31]. Recently [1–4] we found that for naturally occurring ELMs, the phase of the signals from a system scale diagnostic, the toroidally integrating full flux loops in the divertor region of JET, contains statistically significant information on the ELM occurrence times. The signal phases align to the same value on a ~ 2 –5 ms timescale before each natural ELM occurs. This offers a potential direct diagnostic to distinguish pellet triggered ELMs from those that occur naturally.

Here we focus on a JET plasma experiment in which ELMs are triggered by pellets in the presence of ELMs which occur naturally. We use a simultaneous high time resolution Be II signal to determine the ELM occurrence times. We perform

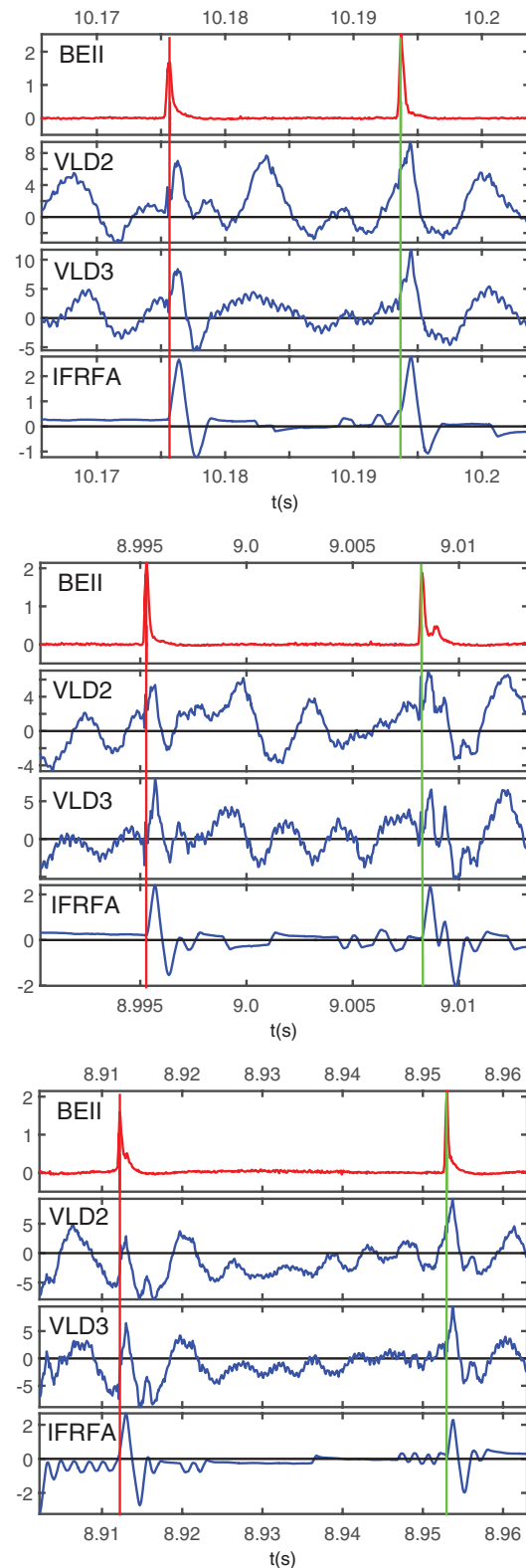


Figure 1. Standardized traces of the raw timeseries for pairs of successive ELMs in JET plasma 86908. From top to bottom, time traces are plotted of: Be II intensity (red); full flux loops (blue) VLD2, VLD3; and fast radial field coil current IFRFA. To facilitate comparison we have standardized the signal amplitudes by dividing by a multiple of their respective means over the flat-top H-mode duration, and then subtracting a local mean so that they are plotted in dimensionless units. The occurrence times of successive ELMs are indicated by vertical red and green lines.

direct time domain analysis of data from two sets of azimuthal coils for which there are high time resolution signals. The first set comprises full flux loops in the divertor region in JET, VLD2 and VLD3, their currents are proportional to the voltage induced by changes in poloidal magnetic flux. The second set is the current in the fast radial field coils (IFRFA), which are actively used for vertical stabilization of the plasma by the control system [33]. Taken together, these capture aspects of both the perturbation from the control system and the active global plasma response. We investigate the time dynamics of the signal temporal analytic phases, and directly test whether these signal phases contain information on the build-up to an ELM. We find that these signals do not clearly phase align before the pellet-triggered ELMs in these signals, whereas they do align for the natural ELMs within the same plasmas. This provides a direct test that can be used to distinguish when an ELM is triggered by a pellet, as opposed to occurring naturally. This result further supports the idea of a global build up phase to naturally occurring ELMs: pellets can trigger ELMs even when the signal phase is at a value when a natural ELM is unlikely to occur.

Since the fast radial magnetic field coils are part of the control system that actively maintains the plasma, our results also support the wider conjecture [1–4] that naturally occurring ELMs are precipitated by coherent global plasma dynamics emerging from nonlinear feedback between plasma and control system. Low amplitude background fluctuations in the active control system field coil current and passive full flux loops could become phase synchronized [38–40], through their individual interactions without the need of coupling between them.

2. Details of the experiment and analysed signals

We focus on one of a series of JET plasmas in which injected pellets were used to precipitate ELMs and where the occurrence frequency of naturally occurring ELMs exceeded that of pellet injection. In JET plasma 86908 the plasma parameters are $I_p = 2.0$ MA, $B_t = 2.1$ T, $P_{NI} = 13$ MW and we analyse ELMs over the interval 9.0–20.7 s.

We analyse two sets of high (100 microsecond) time domain resolution toroidally integrating signals: (i) the current in the fast radial field coils (IFRFA), which are actively used for vertical stabilization by the control system; and (ii) voltages across passive full flux loops (VLD2 and VLD3). The VLD2 and VLD3 signals are the inductive voltage in the full flux loops which circle the JET tokamak toroidally at a location just below and outside the divertor coils, see figure 2 of [32] and also the JET cross section in [3]. They are directly proportional to the current in the full flux loops and hence the divertor rate of change of enclosed flux over the entire torus. These flux loops are passive, in that they input to the control system only. We present analysis of the VLD2 signal, and we repeated the analysis for the VLD3 signal and obtained the same results. The IFRFA signal is the current in the vertical control coils [33] which circle the JET tokamak toroidally and are located at approximately 2/3 of the height of the vessel.

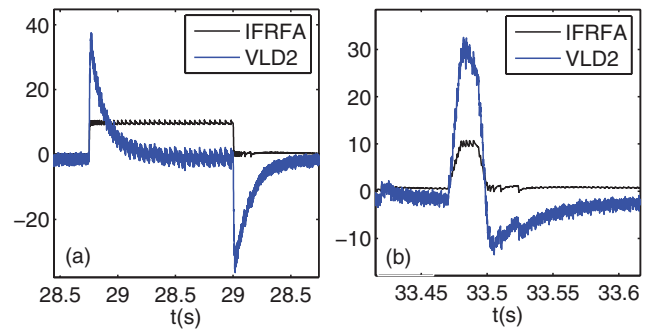


Figure 2. Experiment 87095 on JET where the IFRFA is run through a test sequence with no plasma. The actively pulsed radial field coil (IFRFA, black) and full flux loop response (VLD2, blue) are plotted for two example test signals. These signals are standardised as in figure 1 so that they are plotted in dimensionless units. The full flux loop response can be seen to track fast changes in the radial field coils, there is no observable lag. When the radial field coil current is held constant, the full flux loop has a decay time of ~ 0.2 s.

The IFRFA flux loop is active, in that it both inputs and outputs to the active control system of the plasma.

In plasma 86908 the smallest fuelling size D pellets (cylindrical, diameter 4.0 mm, length 3.2 mm, containing nominally 2.4×10^{21} D atoms) were injected at about 150 m s^{-1} from the torus outboard side at an average rate of 5 Hz. Details of the set-up are in [34]. The pellet injection times are identified by the strong D_α radiation emitted during pellet ablation, lasting for typically 1 ms and recorded by wide angle diodes or fast framing cameras. For all the pellets in plasma 86908, using the Be II peak to define the ELM occurrence time as above, an ELM is found to occur about 1 ms after the pellet burn-out time. We will see that this is approximately the rise time of the VLD and IFRFA signals at the onset of the triggered ELM. Pellet injection impacts the ELM cycle, within ~ 1 ms all pellet particles are deposited in a narrow region close to the plasma edge. This modifies the plasma profiles and transiently alters the power flux into the edge region and can thus prompt the occurrence of the next ELM. To ensure that the pellet is entering a non-perturbed plasma the pellet injection rate is set here to be sufficiently low that the perturbation introduced by a pellet has already decayed when the next pellet arrives [35].

We determine the ELM occurrence times t_k by identifying the peak of the Be II signal within each ELM using the method in [1]. This method does not distinguish ELMs that occur naturally from those that are triggered by pellet injection. We identify pellet triggered ELMs by searching for the first ELM identified by this algorithm that occurs following a pellet.

Sample timeseries of these (standardised amplitude) signals from plasma 86908 are shown in figure 1, over time intervals extending over pairs of successive natural ELMs. The times t_k, t_{k+1} determined by this method are marked with vertical lines on the figure. There is a large bipolar response to each ELM in these signals which then decays away, however the signals continue to oscillate at a lower amplitude throughout the time interval between one ELM and the next. The passive full flux loop signal does not simply track the active fast radial field coil signal. This difference reflects the plasma response;

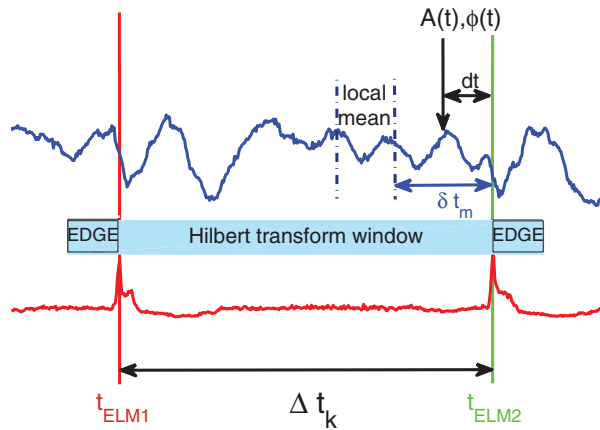


Figure 3. Schematic (not to scale) of the procedure to determine temporal analytic amplitude and phase difference. We first perform a 3 point spline smoothing to remove noise fluctuations on the sampling timescale and then subtract a local signal mean which is obtained in a 7.5 ms sub-window at a time $\delta t_m = 2.5$ ms. This local mean is also used to standardise the signals in figures 1 and 2. The time dependent full flux loop temporal analytic amplitude and phase difference is obtained as a function of the time interval dt measured back from the time $t_{k+1} = t_{ELM2}$ of the second ELM in an ELM pair occurring at t_k, t_{k+1} . Phase difference is calculated w.r.t the temporal analytic phase at the time of the first ELM in the entire sequence ($k = 1$). The temporal analytic amplitude and phase are determined in a time window $\Delta t_k = t_{k+1} - t_k$ within the Hilbert transform window edge which extends 50 ms beyond this.

if the plasma is absent, as shown in figure 2, the passive full flux loops do respond almost instantaneously to changes in the active fast radial field coil current. We will now directly obtain the instantaneous temporal analytic amplitude and phase of these signals in order to test for information in these oscillations.

3. Full flux loop instantaneous temporal analytic phase and build-up to an ELM

A time series $S(t)$ has a corresponding analytic signal defined by $S(t) + iH(t) = A \exp[i\phi(t)]$, where $H(t)$ is the Hilbert transform of $S(t)$, defined in [36, 37, 39] see also [38, 40]. This defines an instantaneous temporal analytic amplitude $A(t)$ and phase $\phi(t) = \omega(t)t$ where the instantaneous frequency is $\omega(t)$ for the real signal $S(t)$. We compute the analytic signal by Hilbert transform over each waiting time Δt_k between each pair of ELMs. The procedure is summarized in the schematic shown in figure 3, which shows the domain over which the Hilbert transform is calculated relative to a pair of ELMs occurring at t_k and t_{k+1} . We will obtain the temporal analytic amplitude and phase for the full flux loop signals for a sequence of times dt preceding the second ELM of each pair, that is, at times $t_{k+1} - dt$. Here, the transform window extends beyond the time of the ELM. We have verified [3] that the phase alignment identified here in the global build up to an ELM can still be identified even if a window is chosen that does not extend to the time of the ELM. Importantly, the phase difference of all the ELMs is defined relative to a single

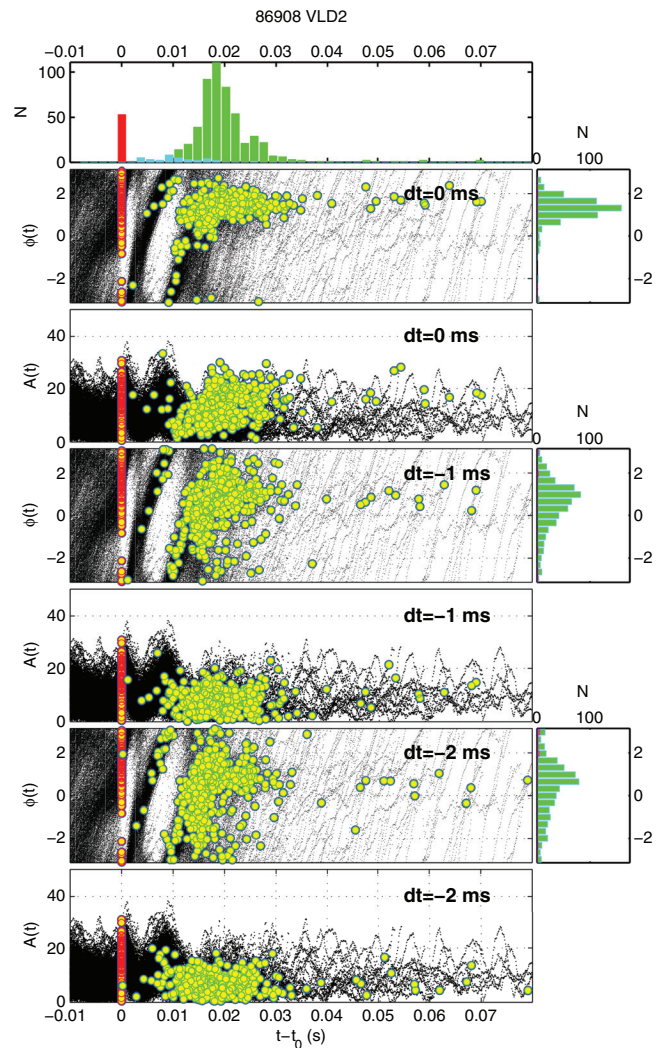


Figure 4. ELM occurrence times and VLD2 temporal analytic amplitude and phase shown for all naturally occurring ELMs in the flat-top of JET plasma 86908. On all the main panels the x -coordinate is time $t - t_0$ (s) elapsed since an ELM. The top panel plots histograms of the time between one ELM and the next, for each pair of successive k th and $(k + 1)$ th ELMs the occurrence time of k th ELM (red) is at time $t_k = t_0$ and the $(k + 1)$ th ELM (green) is at time $t_{k+1} = t$. The frequency N of k th ELM plot has been rescaled by $1/10$. The next pair of main panels (black lines) VLD2 instantaneous amplitude and phase modulo 2π , as a function of time $t - t_0$ (s) elapsed since each ELM up to the occurrence time of the next ELM. The coordinates are amplitude $A(t)$ which is normalised as in figure 1 (dimensionless units) and difference in temporal phase $\Delta\phi = \phi(t) - \phi_0$, where ϕ_0 is the phase at which the first ($k = 1$) ELM in the entire sequence occurs. ELM occurrence times are marked on each VLD2 trace with yellow-filled red circles (k th ELM) and yellow-filled green circles ($(k + 1)$ th ELM). Moving down the figure, the amplitude and phase of the $(k + 1)$ th ELMs are plotted at successively earlier times $t - dt$, that of the k th ELM are unchanged. The right hand panels plot histograms of VLD2 $\Delta\phi(t - dt)$ of all the ELMs.

value, the phase ϕ_0 at which the first ELM ($k = 1$) in the entire sequence occurs.

During chosen plasma H-mode flat top phases there are a few hundred ELMs. Figures 4 and 5 plot how the instantaneous amplitude and phase of the VLD2 and IFRFA signals evolve from one ELM to the next for all the (570) ELMs in the H-mode

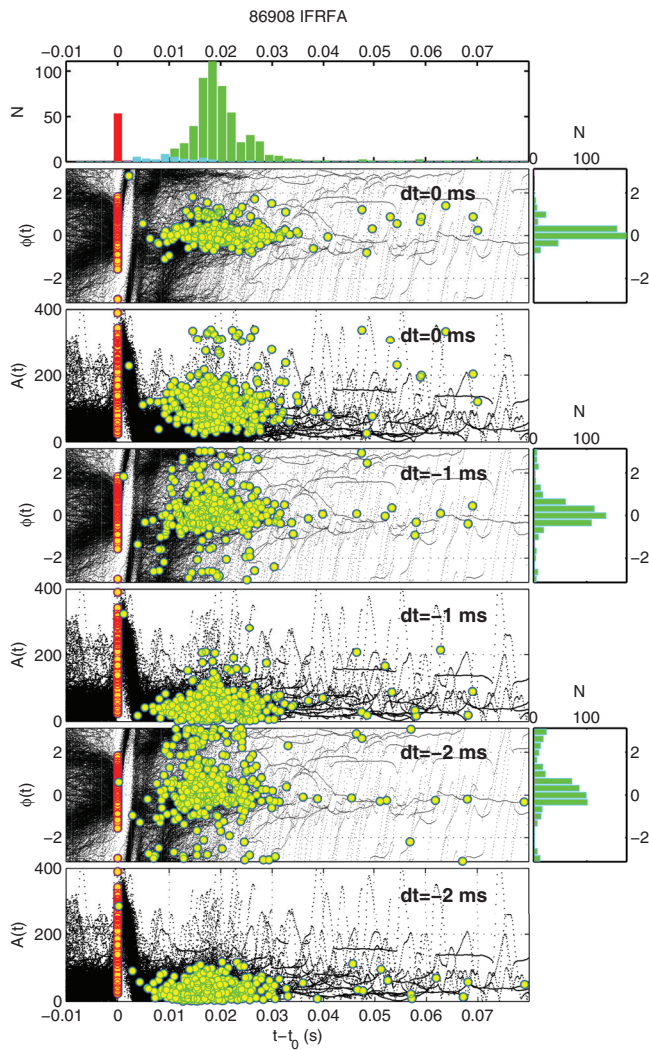


Figure 5. ELM occurrence times and IFRFA temporal analytic amplitude and phase shown for all naturally occurring ELMs in the flat-top of JET plasma 86908. The format follows that of the previous figure.

flat top in plasma 86908. Alternating panels plot instantaneous amplitude and phase versus time. Here, all phases are measured from a single reference, the instantaneous phase of the signal at the time of the first ELM in the H-mode flat top. The phase at the occurrence time of each ELM is plotted at time zero and black traces plot the time evolving phases up to the occurrence time of the next ELM. The green circles plot the phase at time dt before the next ELM occurs, looking earlier in time (more negative dt moving down the plots). We then immediately see that the instantaneous phases are not random, they are phase-bunched. As we move back in time, the phases remain bunched and track back to progressively more negative values. The active fast radial field coil current that directly tracks the coupled control system and the plasma response thus contains within its instantaneous phase the signal of the build up to an ELM. The fact that the passive flux loop also detects such a signal, but does not simply track the signal of the active field coils, suggests that there is a nonlinearly coupled, synchronous dynamics between control system and plasma, as conjectured in [3] and not simply a ‘triggering’ of ELMs by

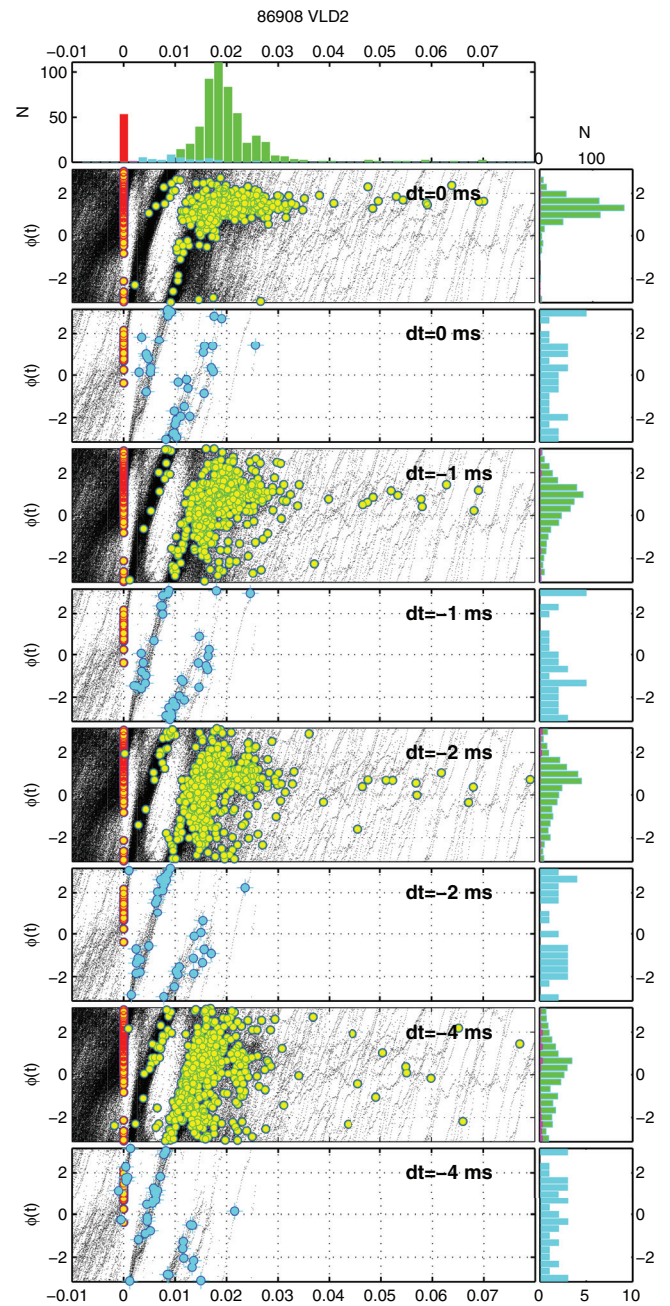


Figure 6. ELM occurrence times and VLD2 temporal analytic phase plotted for the flat-top phase of JET plasma 86908. The format follows that of the previous figure, except that now all naturally occurring ELMs (green) and ELMs that occur following pellet injection (blue) are plotted separately. Note the different scales on the histograms of instantaneous phase plotted in the right hand panels.

the control system. Previously [1] we found evidence of two types of ELMs, prompt ELMs which directly correlate with the VLD2 and 3 response to the preceding ELM, and non-prompt ELMs which occur later, once this response has died away. Both these populations can also be seen in figure 4, the prompt ELMs forming a separate population within $t - t_0 < 0.01$ s and the phase quadrant $+\pi/2 < \phi < +\pi$.

We determine the ELM occurrence times from the Be II emission peak. The start of an ELM can also be seen in the response of the IFRFA and VLD signals. To distinguish

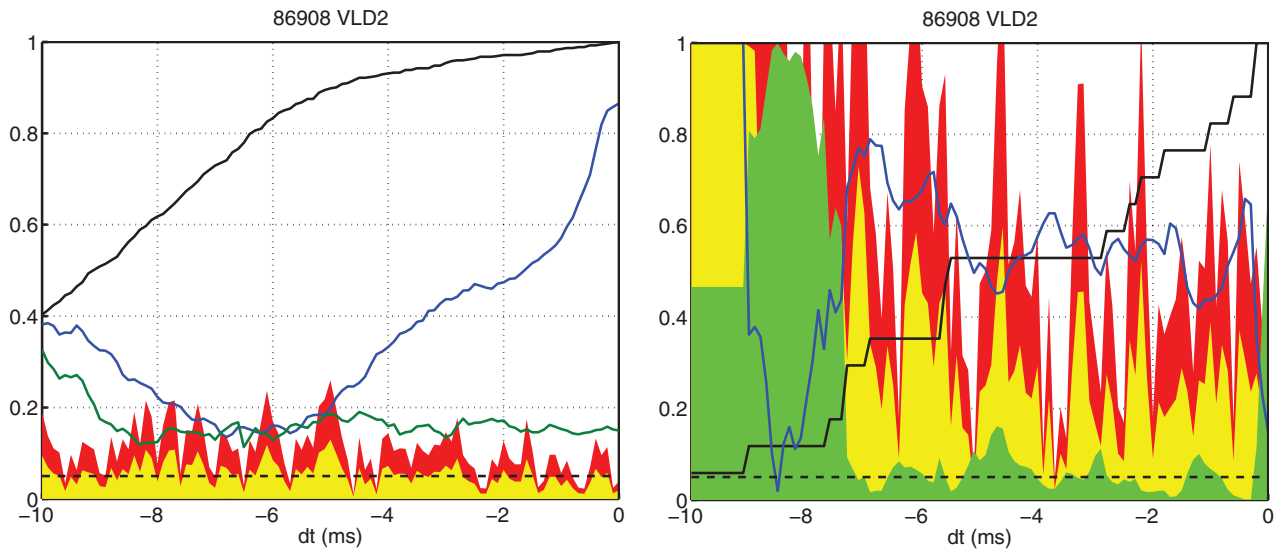


Figure 7. Rayleigh statistics for VLD2 difference in temporal analytic phase $\Delta\phi$ just before an ELM in the flat-top of JET plasma 86908. Left panel is for all natural ELMs and right panel for all ELMs following injection of a pellet. The temporal analytic phase difference is calculated at time dt before the ELM and Rayleigh's R is plotted (y -axis) versus $-dt$ (x -axis). We plot R for the original timeseries (blue line) and two randomised surrogates: (i) the ELM waiting times have been shuffled (green line); (ii) the VLD2 timeseries has been shuffled (yellow shading is the R value and red shading $2 \times R$). The fraction of the total set of ELMs in the analysis is plotted with a black line. The corresponding p -value is indicated by the green filled shading, the $p = 0.05$ level is indicated by the horizontal dashed black line.

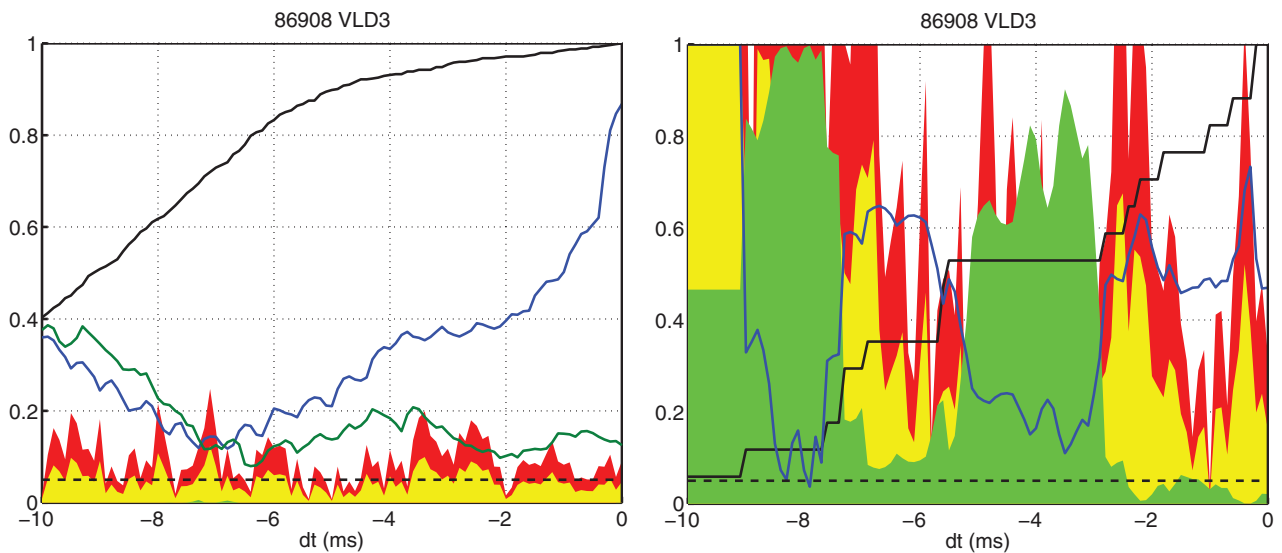


Figure 8. Rayleigh statistics for VLD3 difference in temporal analytic phase $\Delta\phi$ just before an ELM in the flat-top of JET plasma 86908. Left panel is for all natural ELMs and right panel for all ELMs following injection of a pellet. The format is the same as the previous figure.

the IFRFA and VLD sharp rise in response to an ELM from the build-up phase before an ELM, we examine the instantaneous amplitude at, and before, the ELM occurrence time. The rise time of the VLD2 and IFRFA response to the ELM is fast enough that it is possible that these signals are already responding to the ELM by the time the Be II reaches its peak. In figures 4 and 5 we can see that at $dt = 0$, $t = t_{\text{ELM2}}$ (the Be II peak time) the instantaneous amplitude is for some ELMs comparable to the response to the previous ELM. At $dt = -1$ ms before the ELM, the signal amplitudes are for most ELMs closer to the unperturbed level and at -2 ms the amplitudes are generally at the unperturbed level. This confirms that the

response to the ELM in the VLD2 and IFRFA occurs within 1–2 ms just before the ELM time as determined by the peak in the Be II. Before this time, the IFRFA and VLD2 phases are bunched, suggesting that there is an indication of the build-up to an ELM in these global, toroidally integrating signals. We repeated this analysis for the VLD3 signal and obtained the same results.

In figure 6 we have selected, and plotted as a separate population, the first ELM that occurs following the injection time of a pellet which is identified by the strong D_a radiation emitted during pellet ablation. Again, in this figure the x -coordinate is time from the preceding ELM. The ELMs

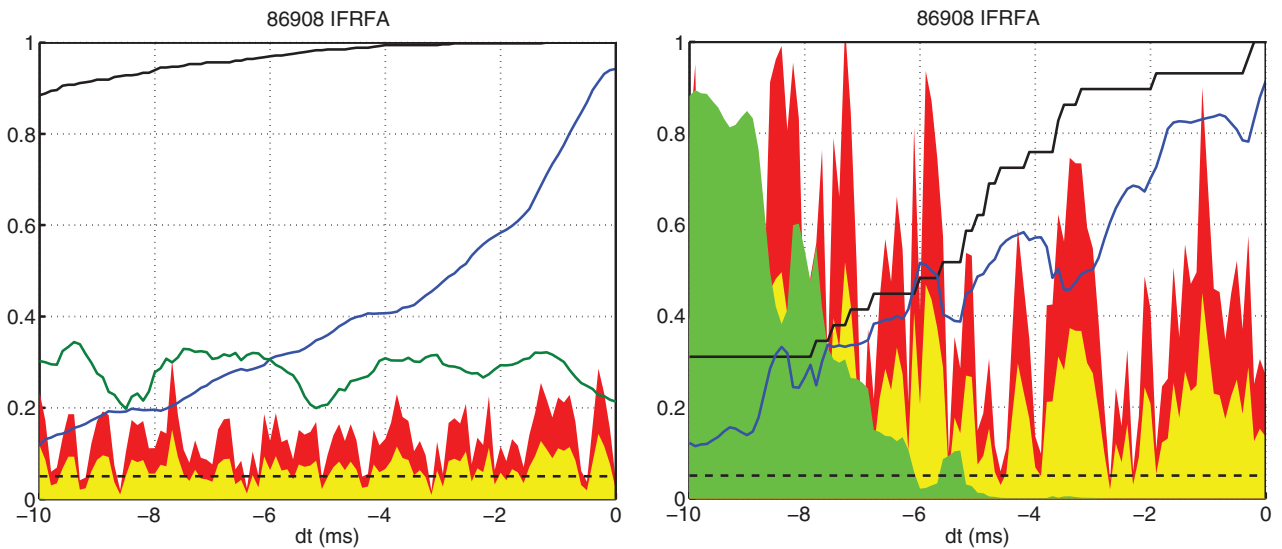


Figure 9. Rayleigh statistics for IFRFA difference in temporal analytic phase $\Delta\phi$ just before an ELM in the flat-top of JET plasma 86908. Left panel is for all natural ELMs and right panel for all ELMs following injection of a pellet. The format is the same as the previous figure.

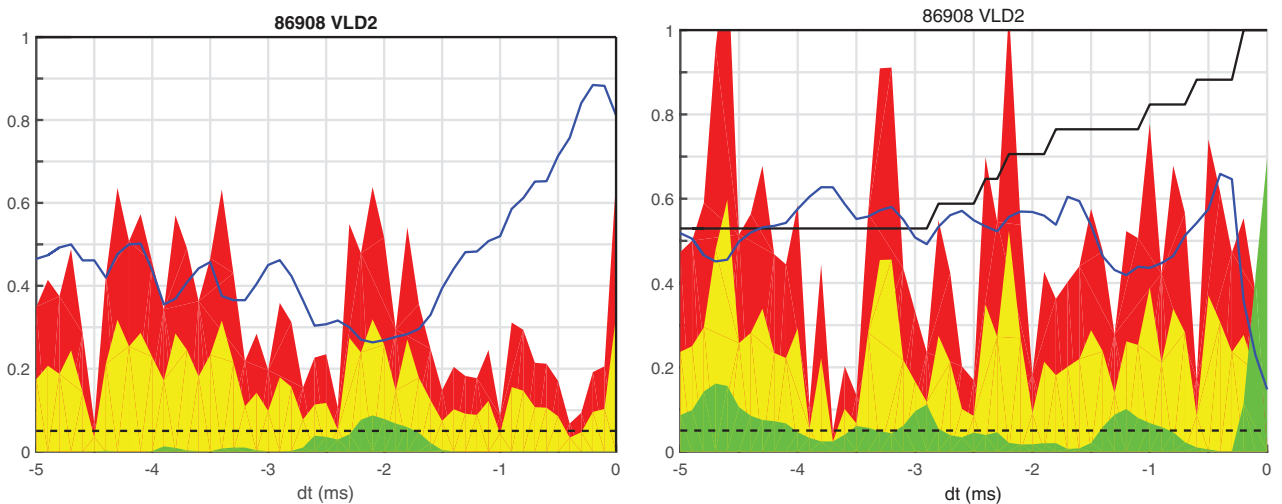


Figure 10. Rayleigh statistics for VLD2 difference in temporal analytic phase $\Delta\phi$ just before an ELM in the flat-top of JET plasma 86908. Left panel is for 35 randomly selected natural ELMs and right panel for all 35 ELMs following injection of a pellet. The format is the same as previous figures except that the time axis is $[-50 \text{ ms}]$.

that closely follow pellets (blue) occur up to 0.02 s after the preceding ELM but more than half of the naturally occurring ELMs also occur within 0.02 s of the preceding ELM. A pellet is injected and then an ELM occurs shortly afterwards but there is a likelihood that this ELM would have occurred even if the pellet had not been injected. Naturally occurring ELMs have distinct behaviour from those that follow pellet injection. Whilst the both the prompt and non-prompt natural ELMs show the phase alignment discussed above, the pellet triggered ELMs do not: they simply occur within 1 ms of the pellet injection time, regardless of the value of the instantaneous phase of the VLD2 signal. This can be seen in the phase histograms on the right hand side of the figure and implies that the pellet triggered ELMs are empirically distinguishable, by this method, from the naturally occurring ELMs. In this plasma the number of ELMs following pellets (35) is much smaller than the total number of ELMs (570),

on the figure these histograms are on different scales. Let us now quantify the statistical significance of the alignment that we have identified.

4. Circular statistics and the Rayleigh test

We use the Rayleigh test (see e.g. [41] and references therein) to quantify the extent to which the temporal analytic phase differences are aligned, and the statistical significance of any such alignment. Using the procedure described above, we determine the temporal analytic phase differences $\Delta\phi_k$ for the $k = 1 \dots N$ ELM pairs in a given plasma. If each temporal phase is represented by a unit vector $\mathbf{r}_k = (x_k, y_k) = (\cos \Delta\phi_k, \sin \Delta\phi_k)$ then a measure of their alignment is given by the magnitude of the vector sum, normalized to N . This is most easily realized if we use unit magnitude complex variables to represent

the $r_k = e^{i\Delta\phi_k}$. Then the Rayleigh number is the magnitude of the sum:

$$R = \frac{1}{N} \left| \sum_{k=1}^N r_k \right| = \frac{r}{N} \quad (1)$$

and if $R = 1$ the temporal phases are completely aligned.

We now check that the above results are significant compared to a random process. First, we construct surrogate timeseries that randomise one property of the timeseries whilst retaining all others. The Rayleigh statistics of these surrogate timeseries are then plotted alongside those of the original timeseries. This analysis of the surrogate timeseries quantifies the likelihood of alternative hypotheses, where phase alignment has occurred by chance. Coincidental phase alignment could arise for example in a finite data-set where both the sequence of ELM arrival times, and the full flux loop signals contain time structure that includes periodicity. This consideration is relevant to the present study, since ELM waiting times have a mean period and the full flux loop signals exhibit intervals of oscillatory behaviour.

Two surrogate timeseries are constructed here: (i) we randomly permute the time sequence of ELM waiting times and (ii) we randomly permute the time order of values in the VLD2,3 and IFRFA signals. For the first of these surrogates, for each ELM waiting time Δt_j we generate a surrogate ELM waiting time Δt_s by selecting at random from the observed time sequence of ELM waiting times $\{\Delta t_1, \Delta t_2, \dots, \Delta t_j, \dots, \Delta t_N\}$, under the condition $\Delta t_s \leq \Delta t_j$. The surrogate set of ELM arrival times that this generates is $t_s = t_{j-1} + \Delta t_s$.

The Rayleigh statistics for the original and surrogate timeseries are plotted in figures 7–9 separately for ELMs that occur following pellet injection and all other, naturally occurring ELMs. An estimate of the $p < 0.05$ value under the null hypothesis that the vectors are uniformly distributed around the circle ([41], see also [3]) is also plotted. A value of $R = 1$ indicates that all phases are exactly aligned, and our random surrogate shows that for the naturally occurring ELMs $R \sim 0.1$ – 0.2 (VLD2,3) and $R \sim 0.1$ – 0.3 (IFRFA) could arise by chance, it is the value obtained by shuffling the ELM occurrence times or the flux loop signals. It follows that that the rise in R -value above 0.3 at $-4 \text{ ms} < dt < 0$ for the real data in figures 7–9 is statistically significant. Whereas the natural ELMs can be seen to progressively align as the ELM occurrence time $dt = 0$ is approached, the pellet triggered ELMs show no statistically significant alignment, they have highly variable values of R and these are comparable to what could occur by chance. For the VLD2 and 3 signals, $p \sim 0.05$ indicating that the null hypothesis of a uniform distribution of phases around the circle cannot be rejected. This is not the case for the IFRFA signal, which is far less sinusoidal in character and hence systematically dwells for longer periods at one or two phase values. However the R value for the IFRFA is comparable to that found for the surrogate timeseries where the signal is shuffled and hence does not indicate statistically significant alignment.

The size of the available pellet precipitated ELM sample (35) is unavoidably significantly smaller than that of the

naturally occurring ELMs (570). The above analysis quantifies statistically significant alignment, or lack thereof, within each sample. One can also compare directly between samples if we fix the sample size to be the same. This is shown in figure 10 where we repeat the above analysis for 35 randomly selected natural ELMs in the plasma, and compare it with the full set of pellet triggered ELMs. We can see that, even in this small sample of naturally occurring ELMs, there is statistically significant phase alignment from about 1.5 ms before the ELM and this is not seen in the same number of pellet triggered ELMs.

We have found that the details of where short-lived fluctuations in R and p -value occur are not robust, they vary with the dataset and with the detailed parameters of how the Hilbert transform is computed. However the overall trends are robust, in particular, alignment of the temporal analytic phases around a single value for dt less than or of order 5 ms for the naturally occurring ELMs.

5. Conclusions

We analysed the signature of the global build-up to ELMs in JET plasmas where ELMs are triggered by pellet injection in the presence of ELMs that are naturally occurring; the natural ELM frequency exceeds that of the injected pellets. We have established a signature of the build-up to naturally occurring ELMs in the temporal analytic phase of high time resolution signals: (i) full flux loops in the divertor region, and (ii) fast radial field coils that are part of the control system that actively stabilizes the plasma. These are toroidally integrating and hence capture global plasma dynamics. Before a natural ELM, the signal phases align to the same value on a ~ 2 – 5 ms timescale. We establish that this global build up to a natural ELM occurs whilst the amplitude of the signals is at its background value; it precedes the response to the onset of ELMing. We perform the same analysis on ELMs which occur following pellet injection and find that these signals do not clearly phase align before the ELM. This result provides a direct test that can be used to distinguish when an ELM is triggered by a pellet as opposed to occurring naturally. It further supports the idea of a global build up phase to natural ELMs. In contrast, pellets can trigger ELMs even when the signal phase is at a value when a natural ELM is unlikely to occur.

Temporal signal phase is always defined relative to some reference value. Here, we have used a single reference phase value for all the ELMs, which is the phase at the time of the first ELM in the entire sequence. In [1, 3], we defined the phase relative to that at the occurrence time of the preceding ELM. Moving from one ELM to the next, the VLD2,3 and IFRFA signal phases are found to lose alignment following the ELM, and then to re-align to the same reference value during the build up to the next ELM. The exceptions to this are the subset of natural ELMs which are prompt [1]; these occur within the VLD2,3 response to the previous ELM and are paced by it. The build up to a non-prompt natural ELM has been identified here in a manner that is independent of

the occurrence time (or instantaneous phase) of the preceding ELM. Phase alignment occurs whilst the amplitude (of the IFRFA, VLD2,3) is small and at a signal phase and time that does not depend on that of the preceding ELM. In particular, the IFRFA is both input and output between plasma and control system. This supports a scenario [2, 3] in which phase synchronization through nonlinear feedback between plasma and control system leads to each non-prompt ELM. This scenario is distinct from an amplitude driven resonance phenomenon in which large amplitude coherent global plasma oscillations pace the ELM occurrence times. In plasmas where conditions are particularly steady and quiescent, the VLD2,3 and IFRFA signal phases may have the same linear dependence on time throughout the H-mode flat top; one could then discern pattern (time-resonances) in the distribution of ELM waiting times, as seen in [30].

Acknowledgments

We acknowledge the EPSRC for financial support. This work has been carried out within the framework of the EUROfusion Consortium and has received funding from the Euratom research and training programme 2014–2018 under grant agreement No 633053. The views and opinions expressed herein do not necessarily reflect those of the European Commission. NWW acknowledges ONR NICOP grant N62909-15-1-N143 and the London Mathematical Laboratory.

References

- [1] Chapman S.C. et al 2014 *Phys. Plasmas* **21** 062302
- [2] Chapman S.C., Dendy R.O., Webster A.J., Watkins N.W., Todd T.N., Morris J. and JET EFDA Contributors 2014 *41st EPS Conf. on Plasma Physics (European Physical Society, 23–27 June 2014)* EPS vol 38F (<http://ocs.ciemat.es/EPS2014PAP/pdf/P1.010.pdf>)
- [3] Chapman S.C., Dendy R.O., Todd T.N., Watkins N.W., Calderon F.A., Morris J. and JET Contributors 2015 The global build-up to intrinsic ELM bursts seen in divertor full flux loops in JET *Phys. Plasmas* **22** 072506
- [4] Chapman S.C., Dendy R.O., Watkins N.W., Todd T.N., Calderon F.A. and JET Contributors 2015 ELM occurrence times in relation to the phase evolution of global measurements in JET *Proc. 42nd EPS Conf. on Plasma Physics (European Physical Society, June 2015)* EPS vol 39E (<http://ocs.ciemat.es/EPS2015PAP/pdf/P2.134.pdf>)
- [5] Keilhacker M. 1984 *Plasma Phys. Control. Fusion* **26** 49
- [6] Erckmann V. et al 1993 *Phys. Rev. Lett.* **70** 2086
- [7] Zohm H. 1996 *Plasma Phys. Control. Fusion* **38** 105
- [8] Loarte A. et al 2003 *Plasma Phys. Control. Fusion* **45** 1549
- [9] Kamiya K. et al 2007 *Plasma Phys. Control. Fusion* **49** S43
- [10] Hawryluk R.J. et al 2009 *Nucl. Fusion* **49** 065012
- [11] Connor J.W. 1998 *Plasma Phys. Control Fusion* **40** 191
- [12] Snyder P.B., Wilson H.R., Ferron J.R., Lao L.L., Leonard A.W., Osborne T.H., Turnbull A.D., Mossessian D., Murakami M. and Xu X.Q. 2002 *Phys. Plasmas* **9** 2037
- [13] Saarelma S., Alfier A., Beurskens M.N.A., Coelho R., Koslowski H.R., Liang Y., Nunes I. and JET EFDA Contributors 2009 MHD analysis of small ELM regimes in JET *Plasma Phys. Control. Fusion* **51** 035001
- [14] Yun G.S., Lee W., Choi M.J., Lee J., Park H.K., Tobias B., Domier C.W., Luhmann N.C. Jr, Donn e A.J.H., Lee J.H. and KSTAR Team 2011 *Phys. Rev. Lett.* **107** 045004
- [15] de la Luna E. et al 2009 *Proc. of the 36th EPS Conf. on Plasma Physics (Sofia, Bulgaria, 29 June–3 July 2009)*
- [16] Lang P.T. et al 2004 *Plasma Phys. Control. Fusion* **46** L31–9
- [17] Sartori F. et al 2008 *35th EPS Conf. on Plasma Physics (Hersonissos, 9–13 June 2008)* vol 32D P-5.045
- [18] de la Luna E. et al 2016 *Nucl. Fusion* **56** 026001
- [19] Lang P.T. et al 1997 *Phys. Rev. Lett.* **79** 1487
- [20] Lang P.T. et al 2002 *Plasma Phys. Control. Fusion* **44** 1919
- [21] Lang P.T. et al 2003 *Nucl. Fusion* **43** 1110
- [22] Lang P.T. et al 2004 *Nucl. Fusion* **44** 665
- [23] Baylor L.R. et al 2013 *Phys. Rev. Lett.* **110** 245001
- [24] Hayashi N. et al 2013 *Nucl. Fusion* **53** 123009
- [25] Pegourie B. 2007 *Plasma Phys. Control. Fusion* **49** R87
- [26] Degeling A.W., Martin Y.R., Bak P.E., Lister J.B. and Llobet X. 2001 *Plasma Phys. Control. Fusion* **43** 1671
- [27] Greenhough J., Chapman S.C., Dendy R.O. and Ward D.J. 2003 *Plasma Phys. Control. Fusion* **45** 747
- [28] Calderon F.A., Dendy R.O., Chapman S.C., Webster A.J., Alper B., Nicol R.M. and JET EDFA Contributors 2013 *Phys. Plasmas* **20** 042306
- [29] Webster A.J. and Dendy R.O. 2013 *Phys. Rev. Lett.* **110** 155004
- [30] Webster A.J. et al 2014 *Plasma Phys. Control. Fusion* **56** 075017
- [31] Murari A., Pisano F., Vega J., Cannas B., Fanni A., Gonzalez S., Gelfusa M., Grosso M. and JET EFDA Contributors 2014 *Plasma Phys. Control. Fusion* **56** 114007
- [32] Murari A., Peluso E., Gaudio P., Gelfusa M., Maviglia F., Hawkes N. and JET-EFDA Contributors 2012 *Plasma Phys. Control. Fusion* **54** 105005
- [33] Neto A. et al 2011 *50th IEEE Conf. on Decision and Control and European Control Conf. (Orlando, FL, USA, 12–15 December 2011)*
- [34] Lang P.T., Frigione D., Geraud A., Alarcon T., Bennett P., Cseh G., Garnier D., Garzotti L., Kochl F. and Kocsis G. 2013 *Nucl. Fusion* **53** 073010
- [35] Lang P.T. et al 2014 *Nucl. Fusion* **54** 083009
- [36] Gabor D. 1946 *Proc. IEEE* **93** 429457
- [37] Bracewell R.N. 1986 *The Fourier Transform and its Applications* 2nd edn (New York: McGraw-Hill)
- [38] Rosenblum M.G., Pikovsky A.S. and Kurths J. 1996 *Phys. Rev. Lett.* **76** 1804
- [39] Pikovsky A., Rosenblum M.G. and Kurths J. 2003 *Synchronization: a Universal Concept in Nonlinear Sciences* (Cambridge: Cambridge University Press)
- [40] Schwabedal J.T.C. and Pikovsky A.S. 2013 *Phys. Rev. Lett.* **110** 24102
- [41] Fisher N.I. 1995 *Statistical Analysis of Circular Data* revised edn (Cambridge: Cambridge University Press)
- [42] Romanelli F. et al 2014 *Proc. of the 25th IAEA Fusion Energy Conf. (Saint Petersburg, Russia)*